韓國海岸・海洋工學會誌
第2卷 第3號, pp. 162～181, 1990年 9月

A Study on Ocean Bottom Coupling Coefficient in East China Sea (a SEASAT-ALT Data Application)

東支那海의 海底摩擦係數의 考察 (SEASAT-ALT 資料의 應用)

Roger Tang*, Byung Ho Choi** and Woo Il Moon***
로저탕* · 崔秉昊** · 文宇一***

Abstract □ The hydrodynamic model is used to analyse the sea surface elevations derived from the SEASAT altimetry over the Yellow Sea and the East China Sea. Periods of significant atmospheric disturbances during the SEASAT mission are selected for this study. These includes periods of July 28-August 2 and August 18-21. Meteorological forcing functions, which are needed for the sea model, are derived by a 2-dimensional grid that is governed by a set of theoretical and empirical meteorological relations over the study area. Ocean tides in this area are known to be significant and introduce a large spatial and time variability in the sea surface elevation. Consequently major tidal constituents of M_2, S_2, K_1 and O_1 are included in the computation. With some knowledge of other known sea surface phenomena e.g.(body tide, loading tide), the time-dependent sea surface variation is predicted to compare statistically with the satellite altimetric measurements and to achieve the objective of ocean bottom friction study. From a total of 10 SEAST orbit tracks, a friction coefficeint was found ranging from 0.0023 to 0.0027.

要 旨: 動水力學模型이 黃海 및 東支那海의 SEASAT 高度計 海面資料를 分析하는데 利用되었다. SEASAT 運用期間中 이 海域에서 颱風이 發生한 7月 28日～8月 2日, 8月 18日～21日 기간이 考慮되었다. 海洋模型에 必要한 氣象外力은 理論 및 經驗的인 關聯式으로부터 誘導되었다. 時空的으로 큰 變化가 있는 이 海域의 海洋潮汐을 算定하기 위해서 M_2, S_2, K_1 및 O_1, 潮汐의 4個分潮가 利用되었으며 地球潮汐의 影響도 고려되어 衛星高度計資料와 統計的인 比較를 위해 時間從屬的인 海面變化를 推定하여 海底摩擦研究를 遂行하였다. 10境遇의 SEASAT軌跡으로부터 調査된 海底摩擦係數는 0.0023～0.0027의 範圍에 있었다.

1. INTRODUCTION

For many years, efforts in geodynamics have been spent on the development of the global ocean tide model (Schwiderski, (1980)), Pekeris and Accad (1969)), the study of the lunar orbit, and the investigation of the variable rotation of the Earth (Munk and MacDonald, (1960), Lambeck (1975)). Most of these problems require some degree of knowledge about the ocean bottom friction and, even more importantly, the understanding of the coupling mechanism between the fluid ocean and the solid earth. In the development of the global ocean tide model, for example, one arrives at the bottom friction term through the integration of the Navier-Stokes equations with the Boussinesq replacement of the Reynolds stress tensor. A certain form of the ocean bottom friction term has to be assumed to

*Texaco Canada Ltd., Calgary, Canada, T2P 2P8.
**成均館大學校 土木工學科(Department of Civil Eng., Sung Kyun Kwan University, Suwon Campus, Suwon, Korea)
***Department of Earth Sciences, The University of Manitoba, Winnipeg, Canada, R3T 2N2.

complete the problem. Another well known examle is the evaluation of tidal dissipation by finding the rate of work per unit surface done by the current at the sea floor. The success of this approach relies on the knowledge of the frictional coefficient (or constant) which links the frictional force at the ocean floor, either linearly or quadratically, with the current velocity. Not only is the frictional coefficient important in these contexts just described, but a variety of storm surge and local ocean tide modelling problems requires a similar dissipation mechanism to integrate the results more accurately (e.g. Heaps (1969)), Tang and Moon (1984), Moon and Tang (1984), Stock (1976), Grace (1930)).

In an earlier study of ocean bottom firction in the area of Hudson Bay by Moon and Tang (1985), a limited range of values of the quadratic friction coefficient (0.0019 to 0.00465) has been derived through the measurement of error between the theoretically computed values and the SEASAT-ALT data at wind speed ranging from 1 m/s to 10 m/s. The sea model algorithm employed was that of the linear shelf model developed by Heaps (1969), Moon and Tang (1984); Tang and Moon (1984). In the present investigation of ocean bottom friction in the East China Sea and Yellow Sea area, different version which includes the modelling of advection phenomena, ocean tide and meteorologically-induced motion is used. This model is employed in conjunction with the well known ocean tidal phenomena in that area and is capable of simulating surge and its interaction with tide. One of the main features in this paper which is markedly different from the previous study is that the investigation is carried out during severe weather condition characterized by wind speed up to 40 m/s. This implies that the propagation of storm surge must be carefully accounted for in that area in order to derive meaningful results. An atmospheric model is required to compute the meteorological forcings prior to the computation of the sea surface response. The 2-dimensional atmospheric model is based on the finite difference form of the geostrophic wind-pressure gradient balance equation. This model operates at some height above the sea model and provides the necessary meteorological driving force as a function

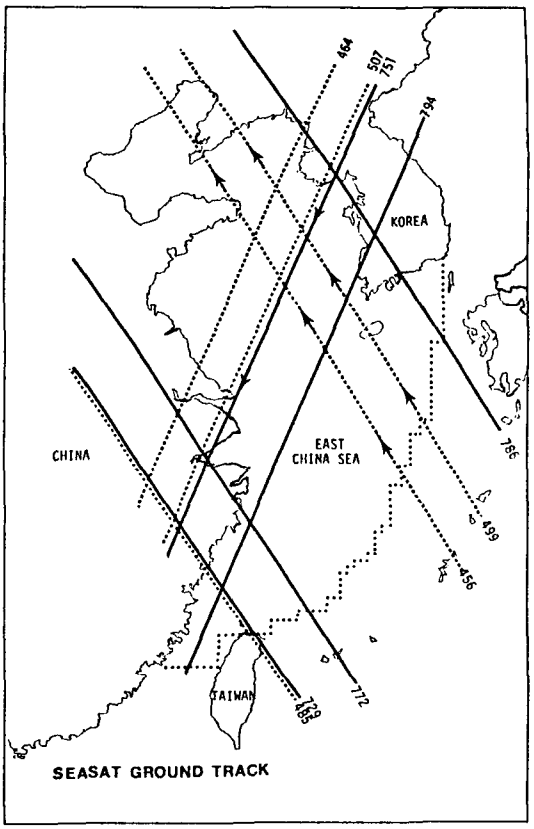

Fig. 1. SEASAT orbit tracks over the area of East China Sea and Yellow Sea during two selected time periods (July 28-Aug 2 and Aug. 12-Aug. 21, 1978).

of time and space in the sea model.

The satellite orbit tracks for the study periods are plotted in Figure 1. These data, including some correction and processing algorithms, were obtained from the U.S. Department of Commerce, Natonal Oceanic and Atmospheric Administration (NOAA). By tuning the ocean bottom friction coefficient in the equation of motion, adjustments of the computed sea surface elevation with respect to the altimeter observations from these passes can be made. This procedure is performed through the use of the time varying sea surface equation (Cartwright and Alcock (1981), Le Provost (1983), Tang (1984). The results of these adjustments allow a set of frictional coefficients to be obtained. This set of values is then subjected to an mean-square-error type analysis to find the optimum value of ocea bottom friction coeffi-

cient, which gives the best agreement between modelled and observed sea surface elevation profiles.

2. TIME DEPENDENT SEA SURFACE EQUATION

The time varying part of the sea surface can be broadly classified into two types based on their periodicity of occurences. The periodical components include the solid earth and ocean tides whereas the transient components are due to the varying sea surface wind and pressure gradient fields. The sea surface height $h'(\chi, \phi, t)$ above the standard ellipsoid (semimajor axis = 6378137m and flattening = 1/298.257) in satellite recording geometry is basically of type (Cartwright and Alcock (1981)).

$$h'(\chi, \phi, t) = h_{or}(\chi, \phi, t) - h_a(\chi, \phi, t) - h_{re} \quad (1)$$

where (χ, ϕ, t) are the spatial and time coordinates, $h_{or}(\chi, \phi, t)$ is the estimated orbital radius of satellite by ground tracking system, $h_a(\chi, \phi, t)$ is the altimeter height after removing instrumental error and atmospheric delay, and h_{re} is the adopted reference (or standard) ellipsoid. This equation is closely approximated by the geoid, plus other known time varying sea surface phenomena (Le Provost (1983), Cartwright and Alcock (1981).

$$G(\chi, \phi, t) + h_b + h_{ot} + h_l + h_s + h_w + h_{pg} + \varepsilon = h'(\chi, \phi, t) \quad (2)$$

where

$G(\chi, \phi, t)$ - geoid above the standard ellipsoid

h_b - body tide of the solid earth

h_{ot} - ocean tide

h_l - ocean induced loading tide of the earth crust

h_s - long wavelength (low frequency) steric variations of the ocean

h_w - sea surface fluctuation caused by wind

h_{pg} - sea surface fluctuation caused by pressure gradient

ϵ - contains unmodelled error of both satellite measurements and the time invariant part of the steric ocean surface set up by quasi-steady currents.

The time varying part of the sea surface T(t) can then be expressed by:

$$T(t) = h_b + h_{ot} + h_l + h_s + h_w + h_{pg} \quad (3)$$

Most of thhe items in the above equaton are given in the SEASAT-ALT GDR except for the effects due to the meteorological forcings which require accurate information of local weather conditions. In continental shelf areas or coastal sea basins, some of these given items are considered to be insufficiently precise for specific application. For example, the two global ocean tide models in the GDR prepared by Schwiderski (1978) and Parke and Hendershott (1980) are primarily for the deeper part of the ocean, and their values in shelf areas may need to be recomputed. In the study of the ocean bottom friction using the SEASAT-ALT data, equation (2), is slightly rearranged as follow:

$$h'(\chi, \phi, t) - G(\chi, \phi, t) + \varepsilon = T(t) + \varepsilon_c \quad (4)$$

where ϵ_c is introduced to represent error in the computation of different components. Equation (4) implies that the altimetric-derived sea surface height with respect to a mean equilibrium signature normally the geoid plus errors in altimeter data processing algorithms, is balanced by the total time varying sea surface heigh with respect to an initial state of rest, with some computational uncertainties.

The variable $G(\chi, \phi, t)$ can be substituted by any existing geoid model, although a locally constructed geoid will be the best to use. In SEASAT-ALT GDR, a fairly accurate geoid surface proposed by the Goddard Space Flight Center is included. The GEM 10B gravimetric geoid was constructed using the global set of GEOS 3 altimeter data with GEM 9 data plus a global set of $1° \times 1°$ surface gravity data. Although this model was completed to a degree and order of 36, it was found to have up to a few meters of error in some area (Marsh and Martin (1982)). These uncertainties are significant since they may be included in the measurements if they were true anomalies. Thus an altimetric-derived reference surface, SS3 surface, is chosen as the equilibrium sea surface in equstions (2) and (4). This means ocean surface is given above the standard ellipsoid and was con-

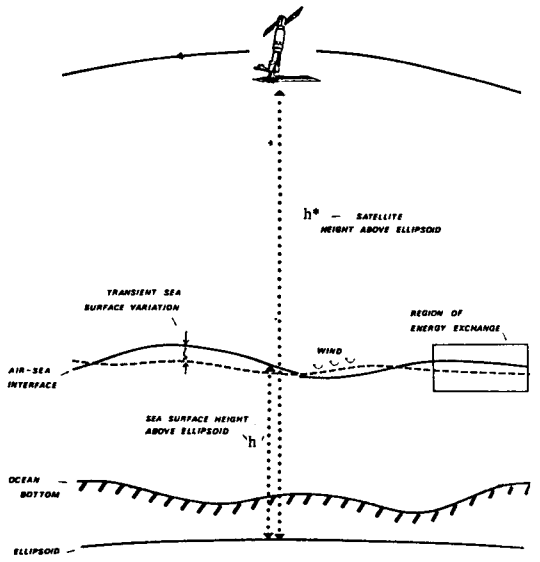

Fig. 2. Geometry of the SEASAT-ALT measurement. h ' is the sea surface height above the standard ellipsoid (defined by semimajor axis 6378.137 km and flattening of 1/298.257) after all corrections have been applied except for the transient effects and the ocean tides.

structed by Marsh and Martin (1982) using the the SEASAT ephemeris calculated by the Preliminary Gravity Solution-SEASAT 3 (PGS-S3) and SEASAT altimeter data from the period 28 July to 14 August. PGS-S3 contains data from GEM 9, SEASAT laser, S band, global gravimetry and GEOS 3 (Lerch et al. (1981)) altimetry. In their analysis, both data sets are combined by accurate gridding techiques to yield global contour maps of the means sea surface topography (SS3). The data of SS3 surface north of 60 degree and south of 63 degree are set to zero due to the possibility of icebergs. This SS3 surface is believed to give a more accurate representation of the equilibrium sea surface than those computed previously (Marsh and Martin (1982), Fu (1983)). Hence, the SEASAT altimeter GDR tape also accompanies the SS3 data set as an alternative reference geoid to the Goddard Earth Model 10B(GEM10B) earth gravity model already adopted for the GDR production. Figure 2 is a schematic diagram showing the SEASAT data collecting geometry.

Equations (2) and (4) are inevitably contaminated by a number of errors which include: (1) the SEASAT ephemeris error which was up to 1.5 m rms, (2) the numerical erros of gridding and interpolation for the production of the SS3 surface, and (3) some unknown systematic erros which can not be minimized by the gridding procedure. Equations (2) to (4) represent all time-dependent sea surface phenomena, as far as they are known, but obviously, the importance of each individual component varies significantly with locality. In the study of sea surface elevations and slopes of the northeast Atlantic Ocean (Cartwright and Alcock (1981), for example, loading tide was completely ignored over the North Sea region, but its effect on open ocean was taken as a constant fraction of the ocean tide. Also, the meteorologically induced sea surface variation was calculated differently for the shelf area and open ocean. In the North Sea and adjacent shelf areas, it was computed by a surge-forecasting model while the same component was estimated by simple hydrostatic law in open sea. Similar simplifications were introduced by Le Provost (1983) in the English Channel where the body tide, loading tide, and steric variations of the ocean were ignored simply because of their small magnitudes compared to other oceanic events.

Employing the gridding technique developed by Schwiderski (1978), the loading tide and body tide were calculated during the two selected mission times to examine their contributions to the sea surface elevation change. As a first attempt, a $0.5° \times 0.5°$ grid was used wit all availble tidal constituents (11 of them). This grid required excess computational time. Thus it was cut down to two $1° \times 1°$ grids for the East China Sea and the Yellow Sea, separately, with the M_2, S_2, K_1 and O_1 tidal constituets. The loading tide in this part of the continental shelf was found to be less than 4.5 cm, a value which is negligible compared to the ocean tide itself. Ocean tide is a well known ocean phenomenon in this area and it dominates all other components in the time varying sea surface equation. The body tide value along the satellite tracks will be presented later, but their effects, similar to the steric variations of the ocean, are also negligible due to their extremely low frequency cha-

racteristic along each orbit track. The largest and smallest magnitude of the body tide are about -12 cm and 3 cm according to the computations. Hence the time varyng sea surface equation can be expressed as:

$$h'(\chi, \phi, t) - G(\chi, \phi, t) = h_{ot} + h_w + h_{\rho g} + \varepsilon_c \quad (5)$$

Before the application of equation (5) which incorporates the corrected SEASAT altimeter data with the model results, short wavelength geoid anomalies have to be investigated over the area. The sea surface height given in GDR is an averaged measurement of 1 sec interval, this is a sampling of a surface distance of 7 km. Therefore, the smallest resolvable wavelength in the measurements along the tracks is approximately 14 km (a distance of 3 consecutive points), according to the Nyquist criteria. Small scale geoid anomalies of the this order could be very important because they can attribute to observations which can not be accounted for in the sea model. The geoid profiles of six up-track and four down-track orbits during the tow selected time periods are shown in Fig. 3. The are mostly characterized by linear functions (extremely low frequency). The possible high frequency components in the geoid were also extracted along the satellite tracks by removing the geoid profiles from the SS3 reference surface profiles. The residual also indicates a low frequency content along the tracks. Thus the geoid, at least along these tracks, is basically long wavelength, and the reduction of the satellite data by a higher frequency reference surface (SS3 surface) should further supress somewhat the small scale geoid anomalies if they exist.

3. OCEAN TIDE AND SURGE MODEL

In the past decade, considerable development has been undertaken on the linear shelf model (Heaps (1969)) and the result is a much improved non-linear version capable of simulating the main tides, surge, and tidal interaction (Heaps (1983)). The major difference between the vertically integrated model and the non-linear version is the inclusion of the advective terms, which have been shown to be important in shallow water bodies (Charnock and Crease (1957)). Including both the atmospheric driving force terms and the non-linear advective terms in the equation of motion, the non-linear version in vector form is given by:

$$\frac{\partial \vec{V}}{\partial t} + \vec{V} \cdot \nabla \vec{V} + 2\omega \Lambda \vec{V} = -g\nabla\zeta + \vec{\tau}_s - \vec{\tau}_B - \nabla \vec{P}_a \quad (6)$$

The equation of continuity is given by:

$$\frac{\partial \zeta}{\partial t} + \nabla \cdot \zeta \vec{V} = 0 \quad (7)$$

where $\vec{V}$ is the vertically-averaged horizontal velocity ζ is the sea surface elevation, ω is the angular speed, g is the gravity acceleration, $\vec{\tau}_B$ is bottom friction term , $\vec{\tau}_S$ is the surface friction due to wind stress, and $\vec{P}_a$ is the atmspheric pressure. The equivalent scalar forms of the equations of motion and con-

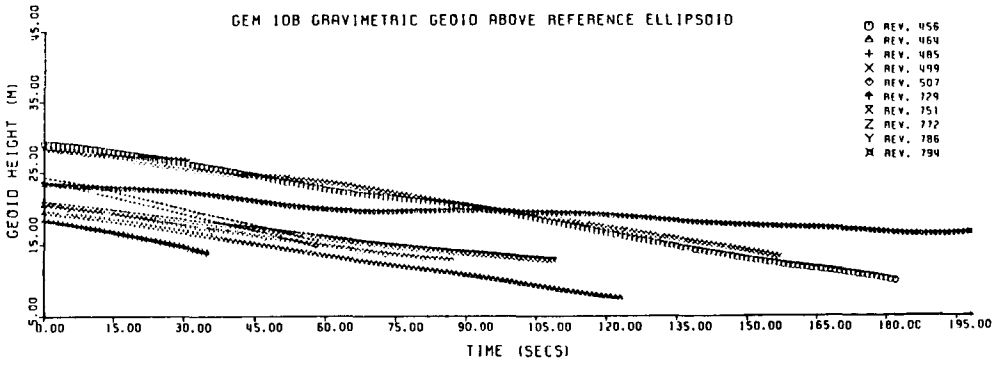

Fig. 3. Six up-track and four down-track geoid profiles from the GEM 10B gravimetric geoid over the East China Sea and Yellow Sea.

tinuity are given by Davies and Flather (1978) and Choi (1980).

These equatios are solved iteratively through time for ζ and $\vec{V}$ starting at an initial state of rest. Because of the capability of handling shallow water effects and modelling of different types of motion, this algorithm has been used for some time in the East China Sea and Yellow Sea continental shelves to study the nature of tides without meteorological input forcings, i.e. pressure gradient and wind stress at the sea surface (Choi, (1980)). Some agreeable comparisons between the model results with a number of measurements conducted across the continental shelf during the joint USA-China Marine Sedimentation Dynamics Study have been reported by Larson and Cannon (1983) and Choi (1983). In this paper, the algorithm is modified to include the meteorological forcing in addition to the original tidal forcing. The tidal constitutents considdred are two semi-diurnal tides (M_2 and S_2) and two diurnal tides (K_1 and O_1). The model results will be utilized to compare with the corrected SEASAT observations to study the ocean bottom friction coefficient in that area.

The mechanism of bottom stress that takes place at the sea floor is not well understood and two alternative representations are acceptable in numerical modelling. If the linear stress law is assumed to be the bottom frictional dissipation mechanism for the transient surge, the bottom stress term is given by:

$$\tau_B = \frac{\eta \rho}{H} \vec{V} \tag{8}$$

where η is the linear stress coeffcient having a typical value of 0.24 cm/s (Weenink, 1958)), ρ is thdensity of the sea water, and H is the water depth. For both surge and tide modelling, the linear law has been demonstrated to be a reasonable approximation (e.g. Grace (1931), Heaps (1969)).

The second and more commonly used alternative of frictional dissipation is to express the bottom stress in terms of the square of the current velocity. This is expressed as:

$$\vec{\tau}_B = \frac{C\rho}{H^2} \vec{V} \ |\vec{V}| \tag{9}$$

where C is the quadratic stress coefficient which traditionally takes values close to 0.003. Although these values have been used in a variety of hydrodynamic modelling with success (Flather and Heaps (1975), Flather and Davies (1978), Choi (1980), whether the particular numerical value used is an optimum one for global ocean or different continental shelf problems has been questionable.

The supply of atmospheric energy and the dissipation of frictional energy in the sea model occur continuously during the computation of the sea elevation, and after a period of time the influence of the intial conditions becomes negligible. To solve equations (6) and (7), the following initial conditions are used:

$$\zeta(\chi, \phi, t) = \vec{V}(\chi, \phi, t) = 0 \quad \text{at } t=0 \tag{10}$$

This condition implies that the sea surface elevation change is generated from an initial state of rest. The sea surface at this state is called the initial state of equilibrium. The coastal boundary condition is give by:

$$V_x \cos\psi + V_\phi \sin\psi = 0 \tag{11}$$

where ϕ denotes the inclination of the normal to the northerly direction and (V_x, V_ϕ) are the components of the depth-averaged current vector.

The finite difference technique used to approximate the nonlinear dynamical equations is the angled derivative method developed by Robert and Weiss (1976). This is an explicit method that relies on the sequential updating of the current values over the grid to evaluate derivatives in the advective terms at each middle time step. The method employed for implementing this experiment is described by Flather and Heaps (1975), Flather and Davies (1978), and Choi (1980). The equations of motion and continuity (equations (6) to (8)) are discretized in time and space using a staggered spatial grid in which the current components are computed at different grid points (Hansen type).

The bottom topography of the model and the discrete water depth values were obtained earlier from various sources (Choi (1980)), Korean Hydrographic

#1262 and #1262 and #2347; and Japanese Hydrographic Charts #182a, #182b, #187, #210, and #302. The open sea boundary of the model is chosen to be bound by a 200 m water depth contour and the entire continental shelf has a typical water depth value of about 80 m.

The grid resolution of the sea model is 0.2 degree in latitude and 0.25 degree in longitude. According to Flather (1972) and Choi (1983), the stability criterion of a linearized version of the scheme in rectangular coordinates is closely approximated by the CFL criterion as follows;

$$\Delta t < \sqrt{\frac{2}{gh}\left(\frac{\Delta x}{2}\right)} \tag{12}$$

where Δx is the grid spacing in Cartesian coordinates and Δt is the time step for the computation.

The above condition gives a minimum time step of 3.75 min. Even though it is obtained from a simplified assumption, it should be treated as a guide for numerical computation.

4. INPUT FORCING FUNCTIONS FOR THE HYDRODYNAMIC MODEL

Tidal forcing

There are several expressions for input tidal forcing depending on the type of modelling and the structure of the numerical scheme. For tide and surge simulation, Davies and Flather (1978) used the following open boundary condition for sea surface elevation in their North Sea model which was previously developed by Davies (1976).

$$\zeta(\chi, \phi, t) = \zeta_m(\chi, \phi, t) + \zeta_T(\chi, \phi, t) \tag{13}$$

where $\zeta(\chi, \phi, t)$ is the surge elevation due to the meteorological influence either observed or computed by simple hydrostatics law at the open boundaries and $\zeta_T(\chi, \phi, t)$ is the part due to tidal motion given by:

$$\zeta_T(\chi, \phi, t) = \zeta_o(\chi, \phi) + \sum_i f_i \tilde{H}_i(\chi, \phi) \cos(\tilde{V}_i + \tilde{\sigma}_i t + \tilde{U}_i - \tilde{g}_i(\chi, \phi)) \tag{14}$$

where

$\zeta(\chi, \phi)$ - mean sea level takin to be zero

f_i, $\tilde{U}_i$ - nodal factors

$\tilde{H}_i(\chi, \phi)$ - the amplitude of constituent i

σ_i - the speed of the constitutent

$\tilde{V}_i$ - the phase corresponding equilibrium constituent at time = 0 at Greenwich

$\tilde{g}_i(\chi, \phi)$ - the phase lag of the tidal constituent behing the equilibrium constituent

Alternatively, the tidal current and surge current can be specified at the open boundaries through the radiation condition used by Flather (1976).

$$q = q_m + q_T + \sqrt{\frac{g}{H}}(\zeta - \zeta_m - \zeta_T) \tag{15}$$

where

q_T - ith constituent tidal current at the open boundary

ζ_T - ith constituent tidal amplitude at the open boundary

q_m - surge current at the open boundary

ζ_m - surge amplitude at the open boundary

The tidal part of the normal current q_T is determined from the following:

$$q_T = \sum_i \tilde{f}_i \tilde{Q}_i \cos(\tilde{\sigma}_i t + \tilde{V}_i + \tilde{U}_i - \tilde{\gamma}_i)) \tag{16}$$

where

$\tilde{Q}_i$ - amplitude of the normal component of the depth-averaged current of constituent i

$\tilde{\gamma}_i$ - phase of the current of tidal constituent i

Equations (13) to (16) supply the tidal forcings to the sea model through the open boundary. Slightly different expressions can be derived from the above conditions in a different type of simulation. For example, Flather (1979) used equations (15) and (16) with only M_2 and S_2 tidal constituents in storm surge modelling whereas Heaps and Jones (1979) and Davies (1976) used exactly the same constituents but employed equations (13) and (14) instead.

Meteorological forcing

The major difficulty of predicting the surface wind speed of a typhoon using the approach of surface wind analysis (Moon and Tang (1984), Tang and Moon (1984), Hsueh and Romea (1983), Heaps

(1983)) has been the lack of an accurate method of converting geostrophic to surface wind speed. From the examination of weather charts obtained from the Korean and Japanese meteorological offices, it is found that not only the weather systems move with an unpredictable speed and direction, but that the pressure gradient near the center of the typhoon may also give unrealistically high geostrophic wind speed. To current the predicted wind speed to typical values of a typhoon, a number of numerical experiments were carried out in this study for the Yellow Sea and East China Sea area.

Several formule for converting geostrophic approximation to surface wind are reviewed and plotted in Figure 4. With those proposed by Hasse and Wagner (1971), four more geostrophic to surface wind relations were tested; the first two of these were modified from Hasse and Wagner (1971), while the last two were derived by Hsueh and Romea (1983) during the wintertime experiment (December 1, 1980 through March 31, 1981) over the East China Sea. The proposals by Hsueh and Romea (1983) were obtained by comparing the geostrophically approximated wind speed from weather charts (supplied by the Japanese Meteorological Agency) with the observations made around the Korean and Japanese coastal stations. Based on a practical stand point and the evaluations of testing results, the following geostrphic wind speed ($|\vec{W}_g|$) to surface wind speed ($|\vec{W}_s|$) conversion equation is adopted for the East China Sea and Yellow Sea area:

$$|\vec{W}s| = 0.443|\vec{W}g| + 2.92 \text{ m/s} \quad (17)$$

The back angle is assumed to be 20 degrees. The adoption of equation (17) is aimed to reduce the magnitude of surface wind and, in addition, the inequality below is added to ensure a realistic range of deduced typhoon wind speed:

$$|\vec{W}s| > 20 \text{ m/s}, \quad |\vec{W}s| = (|\vec{W}s| \pm 20 \text{ m/s}) \times 0.1657 \pm 20 \text{ m/s}$$

where $|\vec{W}_s|$ is the magnitude of sea surface windfield vector derived by the model. The inequality gives a reasonably acceptable pattern of the two dimensional windfield since it suppresses unrealistically high wind speeds near the storm center while it retains nearly normal wind speeds away from it.

The apply the method of extracting wind speed for the East China Sea and Yellow Sea model, an 18×23 atmospheric model grid is set up over the region with a resolution of 1° by 1°. Fig. 5 shows

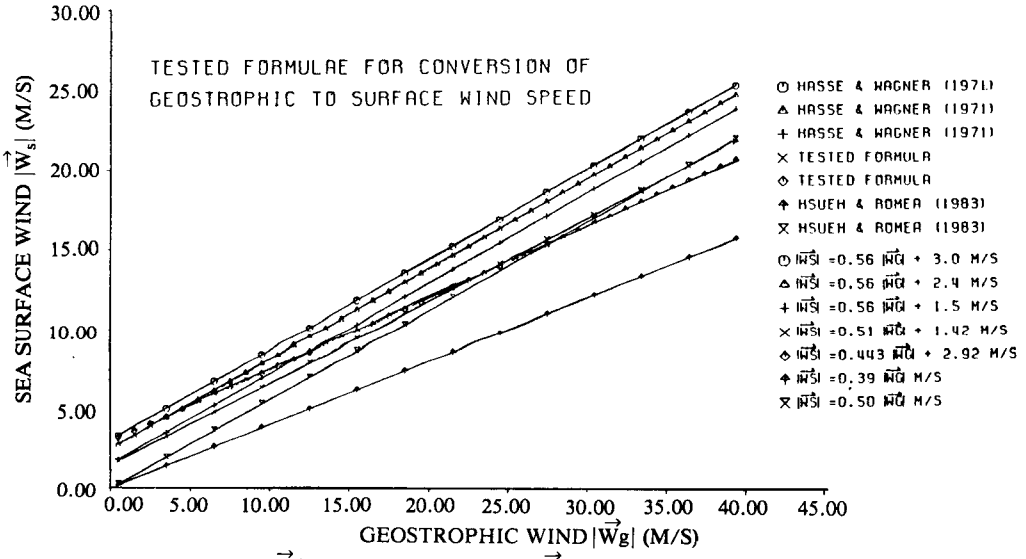

Fig. 4. Geostrophic wind speed ($|\vec{W}_g|$) to surface wind speed ($|\vec{W}_s|$) conversion formulae used in the test runs of the East China Sea and Yellow Sea atmospheric model.

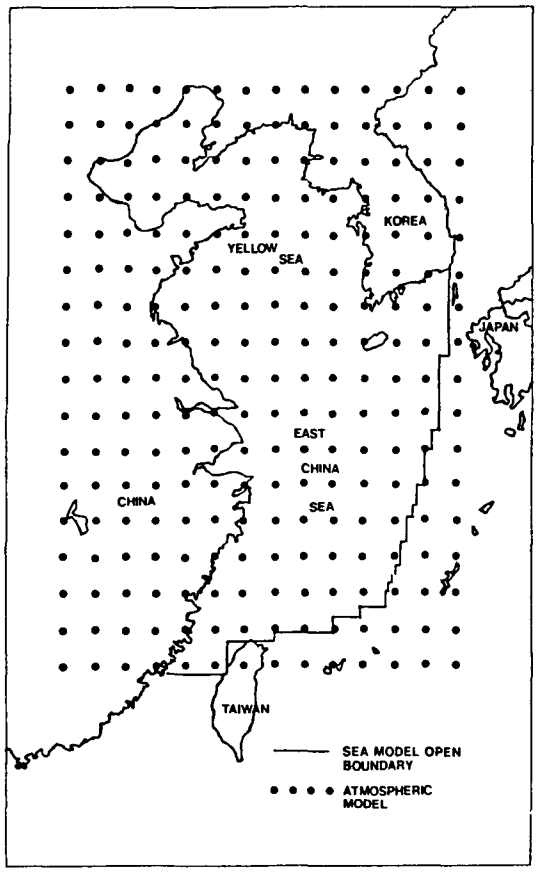

Fig. 5. Some geographical locations of the atmospheric model's grid points. The sea model boundary is shown as solid line segments.

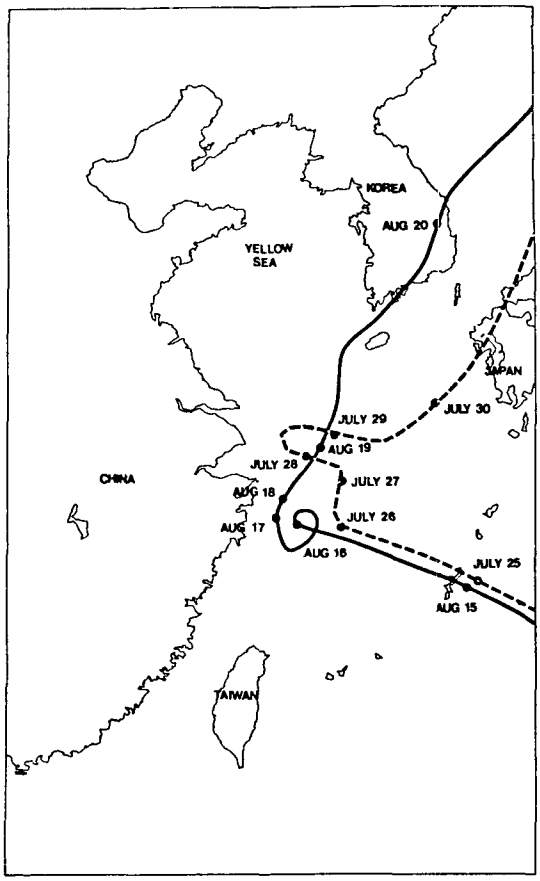

Fig. 6. Traces of the two tropical storms (typhoon): Wendy (dashed line) and Carmen (solid line), during the SEASAT mission time over this area.

some the grid points in and near the study area. A smaller resolution of 0.5 degree (longitude) by 0.4 degree (latitude) was also examined; however, the computation time increases significantly with only a slight improvement in the results.

A total of 13 days of weather (2 periods) is considered over the East China Sea and Yellow Sea area during the SEASAT mission. Each period is characterized by a strong tropical weathe disturbance (typhoon) with a duration of almost 6 days. Fig. 6, depicts the tracks of the typhoons with Wendy (July 28- Aug. 2) as a dashed line and Carmen (August 15-August 21) as a solid line. They enter the sea model at the south-east corner and become stationary over East China Sea region for about 4 days before they move away through the north-east corner of the model (Korea). Since the weather information is collected every 6 hours, it may not be continuous enough to describe the changing weather pattern. Experiences from storm surge modelling in the North Sea and Irish Sea areas (from the research at the Institute of Oceanographic Sciences (10S) at Bidston, UK) show that at least 3-hour intervals of weather input are preferred to produce realistic surge phenomena. Thus interpolation of weather charts in time and space is performed for both periods along the disturbance tracks. This procedure assumes that the typhoons move linearly between two points at which the weather information was made available. A windfield is then recreated evenly along the line defined by these positions at hourly intervals.

Wind stress that inputs into the sea model is com

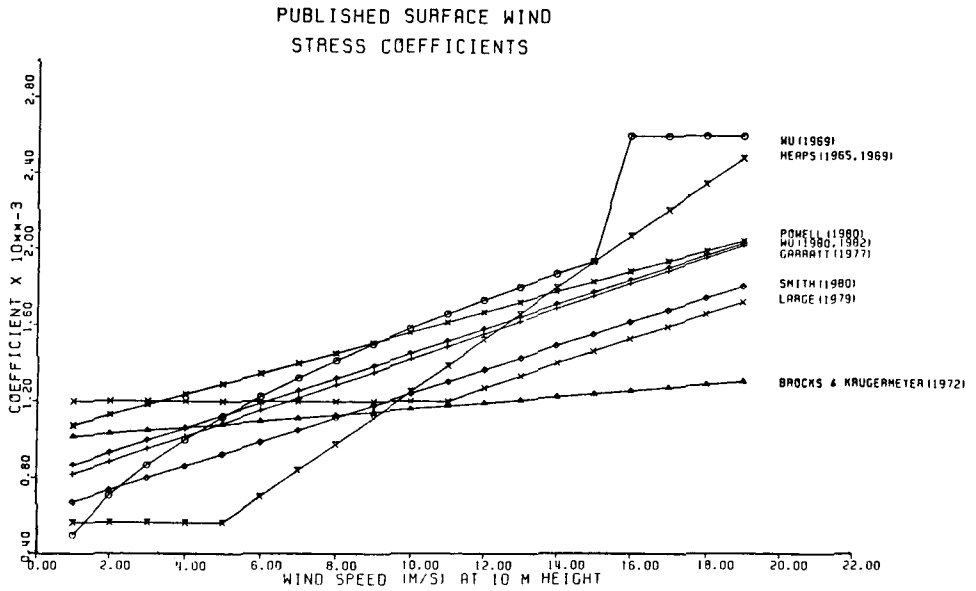

Fig. 7. Plot of surface wind speed to wind stress conversion formulae tested for the sea model.

puted by the standard quadratic law

$$\tau_s = \rho_a C' (|\vec{W}s|)\vec{W}s|\vec{W}s| \quad (18)$$

where ρ_a is the density of air. Various representations of $C'(|\vec{W}_s|)$ (Fig. 7) were numerically examined before the adoption of Wu's proposal (Wu, (1980, 1982)). Previous investigation on the sea surface response caued by wind stress over the Hudson Bay area by Moon and Tang (1984) has also concluded the practical usefulness of Wu's equation during a strong wind environment. This equation is given by Wu (1980, 1982).

$$C' (|\vec{W}s|) = 0.8 + 0.065|\vec{W}s| \quad (19)$$

It is interesting to note that the Powell's relation of wind stress coefficient (Powell (1980)) obtained from hurricane data is quite consistent with Wu's formula at high Wind speeds (Fig. 7). Fig. 8 and 9 show some sample wind stress patterns calculated frm the atmospheric model. Isobars are overlain in each diagram to show the direction of movement.

Since tidal phenomena has been known to be important in this area, ocean tide was calculated separately and also inclusively with surge analysis. Surges in this case have special importance because they were produced by typhoons. Fig. 10(a) through 10(j) show the relative magnitudes of surge, ocean tide, and body tide along the satellite orbit tracks. Ocean tide was generated by 4 major tidal constituents (M_2, S_2, O_1 and K_1) and they have been shown to be sufficient for the reproduction of tide in this region (Choi, (1980)). In general, the variations of ocean tide along the tracks is about 1.75 m with the largest value occurring (in revolution 794) at about 3m. Surge amplitude was smaller according to computation, with a typical value being about 0.5m. The effect of computing surge and tide together may change the shape of these profiles due to the surge and tide interaction. Fig. 11 illustrates examples of the surge plus tide simulation along four satellite orbit tracks using a value of 0.0025 as the quadratic friction coefficient. Also plotted in this diagram are the DC corrected residual sea surface elevation profiles (dashed lines) obtained by subtracting the SEASAT observations from the SS3 altimetric-derived reference sea surface. The amount of DC shifting for each orbit track is computed by the difference between the satellite observed value and the computed value at the mide-point of the profile. This point corresponds to the time when the simulated profile was produced. Comparing the surge and tide

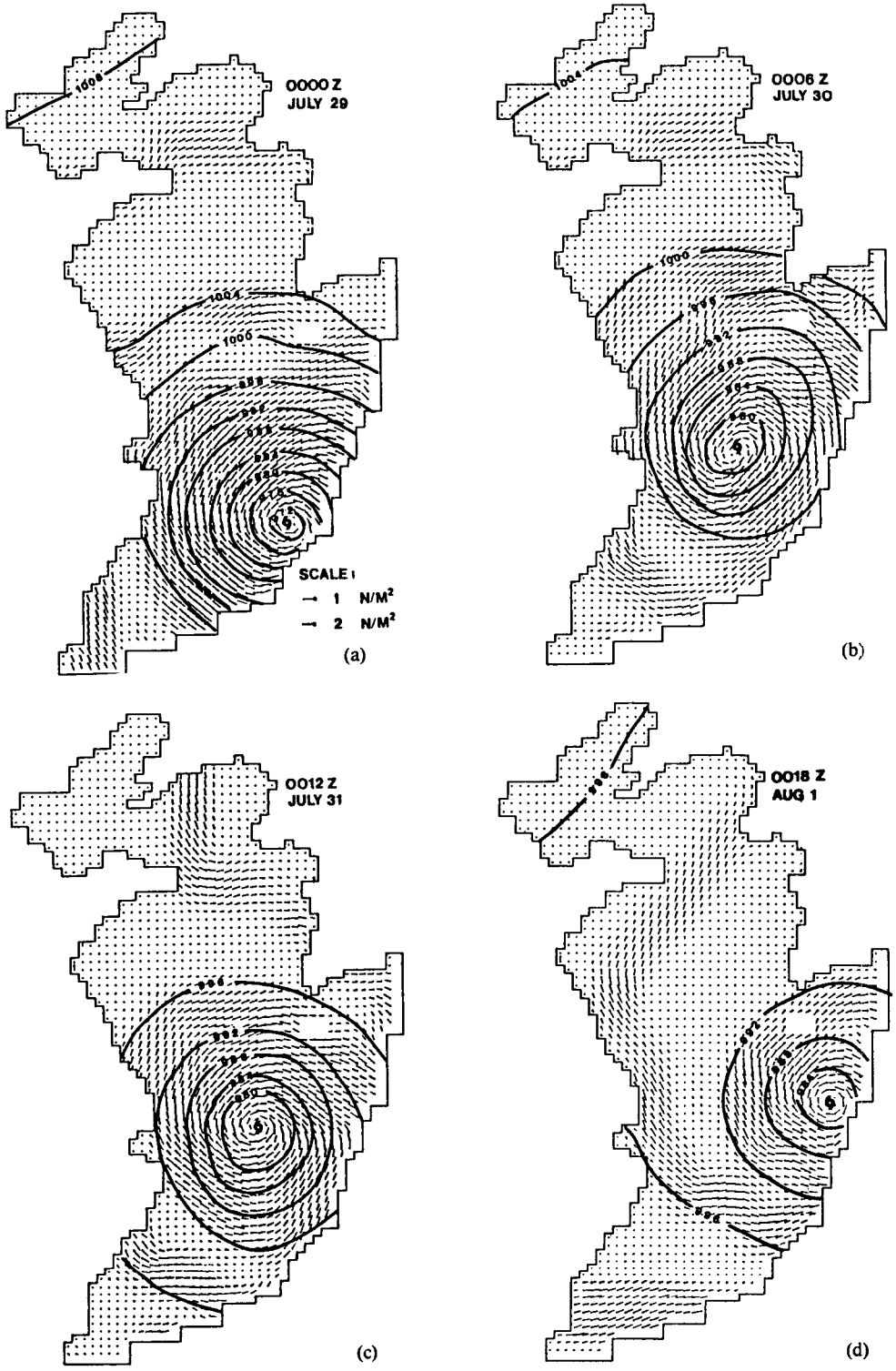

Fig. 8. Samples of wind stress patterns as the results of typhoon Wendy over the East China Sea and Yellow Sea. (a) July 29, 0000Z, (b) July 30, 0006Z, (c) July 31, 0012Z, and (d) Aug. 1, 0018Z.

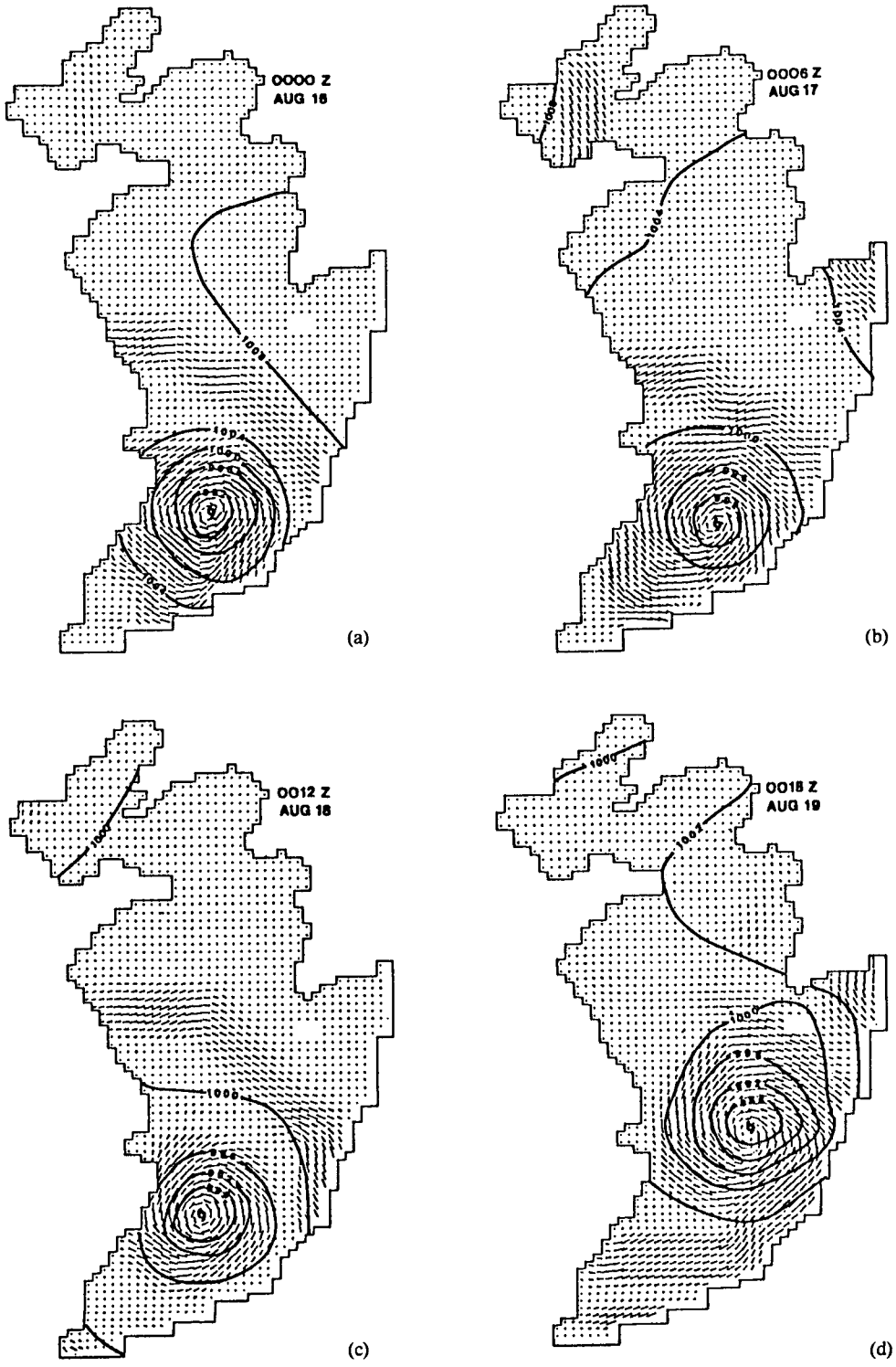

Fig. 9. Samples of wind stress patterns as the results of typhoon Garmen over the East China Sea and Yellow Sea. (a) Aug. 16, 0000Z, (b) Aug. 17, 0006Z, (c) Aug. 18, 0012Z, and (d) Aug. 19, 0018Z.

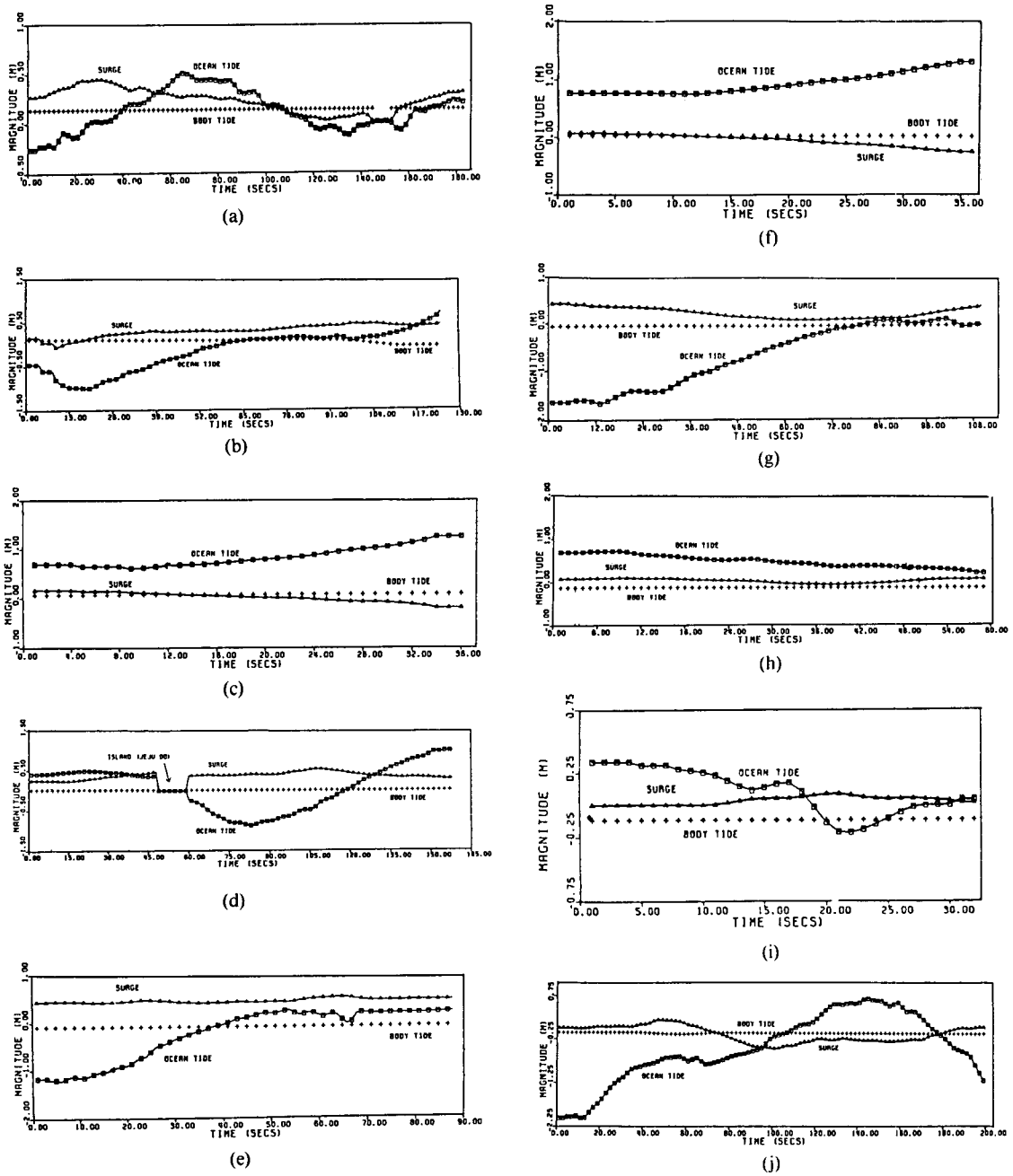

Fig. 10. Magnitude of ocean tide, storm surge and body tide along the satellite profiles shown in Fig. 1. (a) Revolution 456, (b) Revolution 464, (c) Revolution 485, (d) Revolution 499, (e) Revolution 507, (f) Revolution 729, (g) Revolution 751, (h) Revolution 772, (i) Revolution 786, and (j) Revolution 794.

simulations with the results shown in Fig. 10(a) through 10(j), suggests that the sea surface topography (surge + tide) along the tracks is associated with the feature which has the largest relative magnitude, that is the ocean tide. The surge profiles modify the profiles of ocean tide slightly by adding to them with a small residual, probably, caused by some interaction. It is also obvious from Fig. 10(a) through

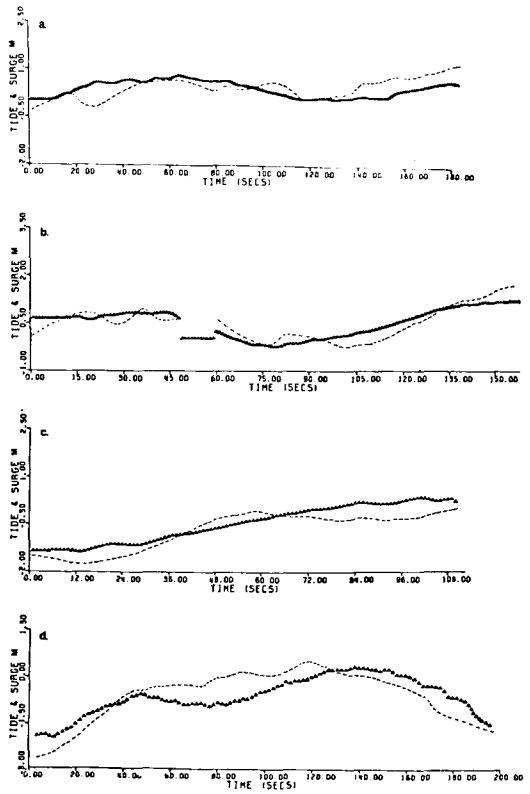

Fig. 11. Diagram showing the results of surge and tide simulations (solid triangles) taking into account their interactions. Dashed lines are the residual DC shifted sea surface elevation profiles obtained from the SEASAT-ALT data after removing from them the SS3 reference sea surface.
(a) Revolution 456, (b) Revolution 499, (c) Revolution 751, and (d) Revolution 794.

10(j) that low frequency, small magnitude body tides along the satellite tracks cause negligible vertical shifts of the profiles when they are subtracted for correction, and thus they can be safely ignored.

5. QUADRATIC FRICTION COEFFICIENT OF THE OCEAN BOTTOM

In general, the expression for the bottom friction law must satisfy the following criteria:

(1) It should give a reasonable magnitude of bottom stress in shallow water (less than 1m), since both the linear and quadratic laws approach infinity

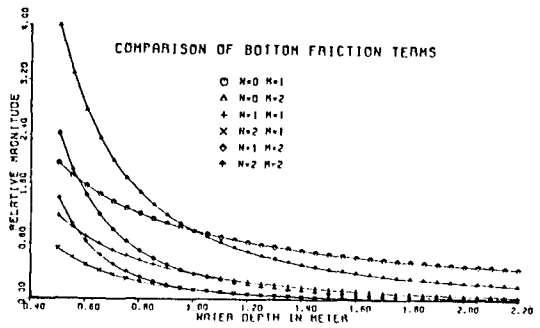

Fig. 12. Graphical representation of the relative magnitude of Equation (20) as a function of water depth.

nearly exponentially as the depth approaches zero.

(2) It must be computationally simple to use. A complex expression may be physically unrealistic in practice. Furthermore, a suitable representation should somehow vary with water depth, an important control parameter.

(3) It should be compatible with the conventional bottom friction laws (i.e., the linear or quadratic friction laws, as the water depth increases).

Given these conditions, the following generalization for the ocean bottom friction term can be used (Kinsman, (1965); Ramming (1978)).

$$\tau_B = a_o \frac{e^{-NH}\rho}{H^M} \vec{V}^M \tag{20}$$

where M = 1 or 2 and N = 0, 1, 2,···. Th parameter M denotes the selection of firctional law with $\vec{V}$ corresponding to the magnitude of depth-averaged current. The parameter N denotes the selection of the damping effect in shallow water and a_o is a constant with or without dimension depending upon the selections. For N = 0, the generalized bottom friction law of equation (20) reduces to the familiar linear and quadratic friction laws for M = 1 and 2, respectivelyy (equations (8) and (9)). In these cases, a_o becames the linear stress coefficient and quadratic stress coefficient, accordingly. To see the behavior of the generalized law in shallow water, equation (20) is plotted for a few combinations of N and M against the water depth H, assuming both the current and the constant to be unity (Fig. 12). From this diagram, it is evident

Table 1. Values of quadratic friction coefficients for bottom friction process.

Author	Frictional Coefficient	Area
Grace [1930]	0.003	*Gulf of Suez*
Bowden & Fairbairn [1952]	0.0036	Red Wharf Bay, Anglesey
Bowden & Fairbairn [1956]	0.0024	Red Wharf Bay, Anglesey
Bowden *et al.* [1959]	0.0035	Red Wharf Bay, Anglesey
Charnock [1959]	0.0034	Red Wharf Bay, Anglesey
Sternberg [1968]	0.0031	Puget Sound, Washington
Hearthershaw [1976]	0.0015-0.0019	Irish Sea
Stock [1976]	0.0015	Gulf of California
Wolf [1980]	0.0014-0.0271	Northern Irish Sea
Weatherly & Wimbus [1980]	0.0056	Blake-Bahama Outer Ridge
Chriss & Caldwell [1982]	0.0032-0.008	Oregon Shelf
Bowden & Fergurson [1980]	0.0040-0.0047	Eastern Irish Sea
Moon and Tang [1985]	0.0019-0.0046	Hudson Bay, Canada
Tang *et al.* [1990]	0.0023-0.0027	East China Sea and Yellow Sea (this study)

that the functions 1/H (linear friction) and 1/H**H (quadratic friction) which are associated with depth-averaged current are not suitable for shallow water (e.g. from 0.6m to 1.2m). However, the magnitudes predicted by various values of N and M uniformly converge to a consistent value as the water depth increases. In general, the addition of the inverse exponential function exp(-NH) in equation (20) reduces the magnitude of the bottom stress when the water depth approaches zero. If the water depth field in the modelling area is restricted similarly to the number given in the figure, equation (20) with N = 1 or 2 would be adquate to minimize the instability of the hydrodynamic solution in shallow water. Further practical experiments have to be carried out to examine other treatments of the bottom friction defined by equation (20). This will require proper insitu measurements in coastal water areas. Further complications arise if the coefficient a_o in equation (20) is no longer simply a constant. From the experiences with the sea surface wind stress coefficient, one may assume that a_o may vary with current (for example, a linear proportionality of a_o to current speed). This is itself a very complicated matter to be studied with our present knowledge, although the possibility does exist for further experiment. The proposal of equation (20), however, overcomes the problem of shallow water and converges to usual friction law when water depth increases. Table 1 summarizes some of the earlier as well as recent works done on the estimation of the quadratic friction coefficient (N = 0, M = 2).

Most of these values are derived from the tidally-induced current observations through a combination of the quadratic stress law with one of the other methods, such as the velocity profile technique or the Reynold stress method. These values are largely confined by the number of measurements, so they can not be regarded as reliable representations. From Table 1 it is clear that the consistency of the quadratic friction coefficient is not satisfactory, although the values obtained from the Red Wharf Bay indicate a small deviation and fall in a range near the traditional value of 0.003. Our confidence with regard to the derived value can only be improved by increasing the number of observations and by extending the experiment to different areas with a consistent approach.

Only the quadratic friction term is a tested in this area simply because the nonlinearity of the term is consistent with the sea model formulation (advection) and other phenomena such as the influence of nonlinear interactions among the tidal constituents. With the quadratic fricton dissipation implemented in the equation of motion, the SEASAT-ALT data and the model results during the selected time periods are subjected for analysis through a function defined

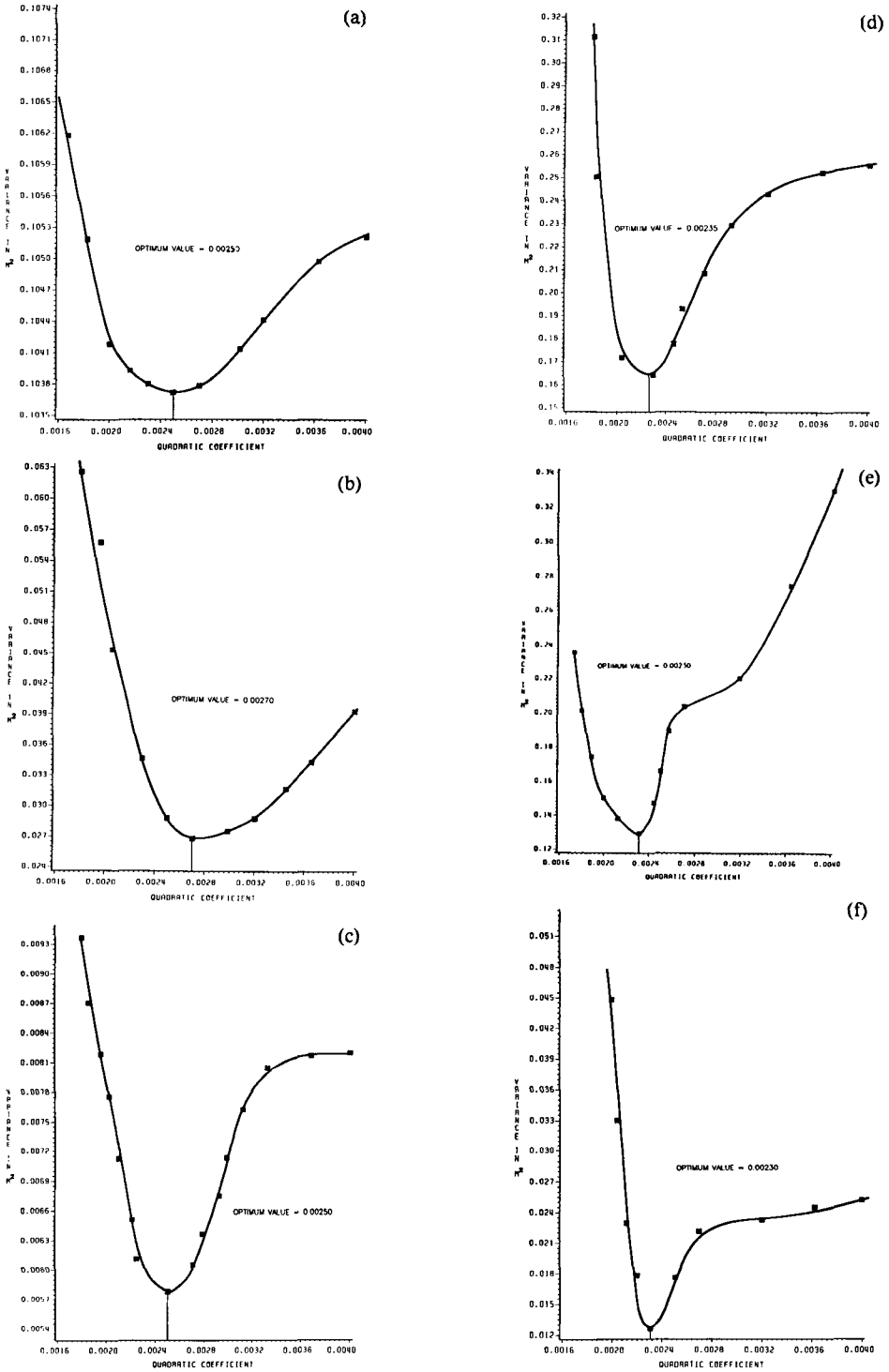

Fig. 13. East China Sea and Yellow Sea Experiment Variance Curves calculated from the observed and simulated sea surface profiles as a function of quadratic friction coefficient.
(a) Revolution 456, (b) Revolution 464, (c) Revolution 485, (d) Revolution 499, (e) Revolution 507, (f) Revolution 729, (g) Revolution 751, (h) Revolution 772, (i) Revolution 786 and (j) Revolution 794.

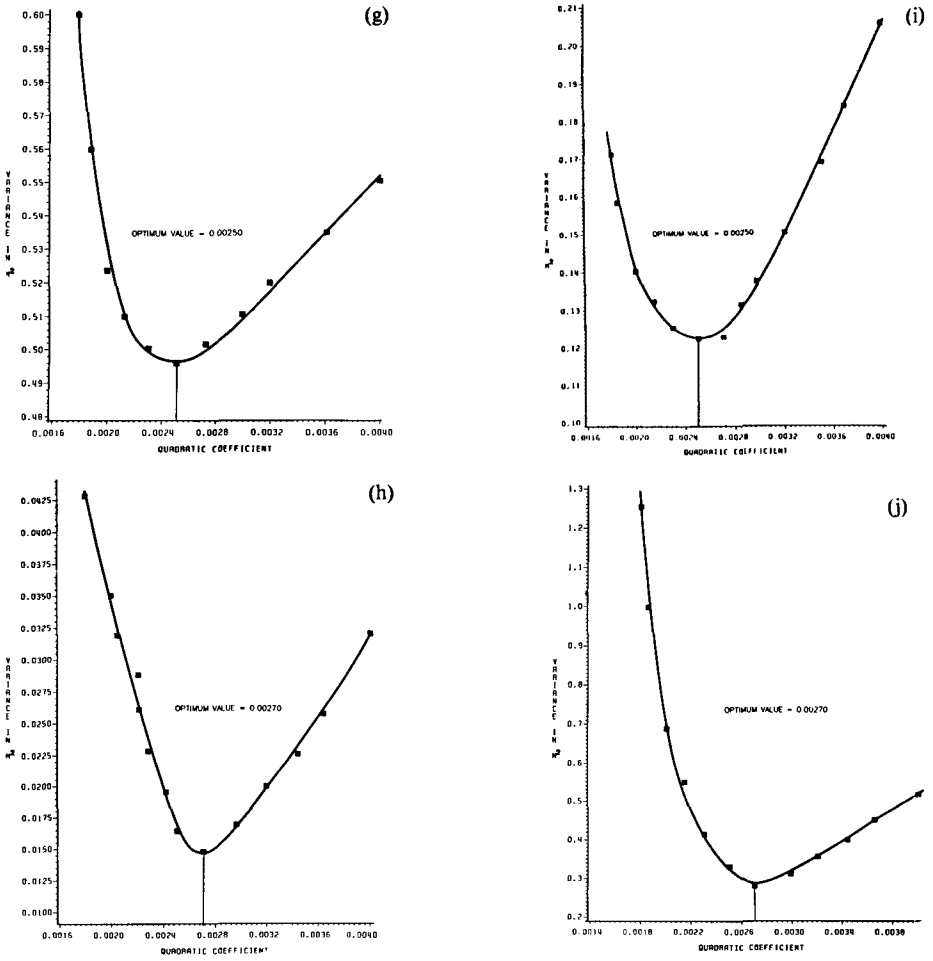

Fig. 13. (Continued)

by Tang (1984):

$$\mathrm{Var}_i\,(C) = \frac{1}{N}\sum_{j=1}^{N} |\zeta_c^j\,(C) - \zeta_{oB}^j\,(\hat{C})|^2 \qquad (21)$$

where

Var_i (C)-variance function for the ith orbit track

C-experimental quadratic friction coefficient

$\hat{C}$-optimum value of C when Var_i (C) is minimized

N-number of recording points along the orbit track

ζ_c^j-computed sea surface elevation profile of ith orbit track

ζ_{OB}^j-observed sea surface elevation profile of ith orbit track

The optimum frictional coefficient C in equation (21) is assumed to be the truth value that gives rise to te satellite recordings. Ideally, the optimization procedure can be carried out using equation (5) which links the satellite data collecting geometry with the sea model coordinates. It is, however, that the long wavelength unmodelled error in orbit computation due to insufficient accuracy in the gravity model and radom noise are excluded. Since the unmodelled error is in general long wavelength of semi-cyclic per revolution (Marsh and Williamson, (1980)), it would

only have an effect on local 'DC' shifting in the SEASAT-ALT data segments such as those used in this research. In fact, 'DC' shifting can also be true for other uncorrected long wavelength small amplitude anomalies of tidal loading of the solid earth, body tide, and steric ocean variations.

The variance curves (Var_i (C)) for the correlation between the model and the altimeter derived observations for each revolution are displayed in Fig. 13(a) through 13(j). The results of the optimization are very consistent with each other within a range of values from 0.0023 to 0.0027. An averaged value is obtained to be 0.002505 for the friction coefficient of the quadratic law.

6. CONCLUSIONS

The quadratic ocean bottom friction law has been examined in the East China Sea and Yellow Sea area through numerical modelling and optimization procedures, in which various frictional coefficients were used in the equation of motion. The variance functions computed by measuring the error between the satellite observations and the theoretical values show surprisingly good agreement. From a total of 10 orbit tracks during two tropical storm periods, a range of quadratic coefficient between 0.0023 and 0.0027 was obtained. The correlation between the satellite measurement and the modelling conclusively show consistency of the estimated friction coefficient close to the conventionally adopted value of 0.0025.

The small range of coefficients obtained in this paper has several important meanings. Firstly, it indicates the effectiveness of the modelling technique which is capable of handling ocean tide, storm surge, and (possibly) their interaction simultaneously. This thereby allows an accurate comparison with the satellite data to estimate a value for the quadratic friction coefficient. Secondly, it implies the validity of the empirical relations used to predict surface wind speed and wind stress. These relations appear to be able to produce reasonable and practical estimations of the magnitude of wind speed for the sea model. Finally, it shows some indications of qualitative improvements in the signal to numerical noise ratio (modelling accuracy) when the surface wind speed or stress increases. This is supported by the earlier investigations in Hudson Bay (Moon and Tang (1984), Tang and Moon (1984)) during which the range of coefficients was found to be larger in a calm to moderate wind speed (1 m/s to 10 m/s) environment.

ACKNOWLEDGEMENTS

We would like to thank Dr. E. Schwiderski for making the Global Ocean Tide Tape available.

REFERENCES

Bowden, K.F. and Fairbairn, L.A., 1952. A determination of frictional forces in tidal current. *Proc. Roy. Soc.*, **A214:** 371-392.

Bowden K.F. and Fairbairn, L.A., 1956. Measurements of turbulent fluctuations and Reyonolds stresses in a tidal current, *Proc. Roy. Soc.*, **A237:** 442-438.

Bowden, K.F. and Ferguson, S.R., 1980. Variation with height of the turbulence in the tidally-induced bottom boundary layer, in Marine Turbulence, ed. Nihoul, J.C.J., Elsevier Oceanography Series, 28.

Bowden, K.F., Fairbairn, L.A. and Hudges, P., 1959. The distribution of shearing stress in a tidal current, *Geophys. J.R. Astro. Soc.*, **2:** 288-305.

Brocks, K. and Krugermeyer, L., 1972. The hydrodynamics roughness of the sea surface, In Gordon (e.d.) Studies in Physical Oceanography, 1, 75-92.

Cartwright, D.E. and Alcock, G.A., 1981. On the precision of the sea surface elevations and slopes from SEASAT altimetry of the northeast Atlantic Ocean, Oceanography form Space, e.d., Gower, J.F.R., Plenum Publishing Corporation.

Charnock, H., 1959. Tidal friction from current near the North Sea bed, *Geophys. J.R., Astrol. Soc.*, **2:** 215-221.

Charnock, H. and Crease, J., 1957. North Sea surges, *Sci. Prog. London*, **45:** 494-511.

Choi, B.H., 1990. A tidal model of the Yellow Sea and the Eastern China Sea, Korea Ocean Research and Development Institute (KORDI), rep. 80-02.

Choi, B.H., 1983. Mathematical modelling of tides and surges in the East China Sea, Paper presented in the International Union of Geophysics and Geodesy, Hamburg, West Germany, 1983.

Chriss, T.M. and Caldwell, D.R. 1982. Evidence for influence of form drag on bottom boundary layer flow, *J. Geophys. Res., G.R.*, **98:** 4148-4154, 1982.

Davies, A.M., 1976. Application of a fine mesh numerical model of the North Sea to the calculation of storm surge elevations and currents, Rep. Inst. Oceanogr. Sci., No. 28, p. 30.

Davies, A.M. and Flather, R.A., 1978. Applications of nu-

merical models of the north-west European continental shelf and the North Sea to the computation of the storm surges of November to December, Dt. hydrogr. Z. Erganzungsheft, A., No. 14.

Flather, R.A., 1972. Analytical and numerical studies in the theory of tides and storm surges. Ph.D. thesis, University of Liverpool.

Flather, R.A., 1976. A tidal model of the north-west European continental shelf, *Mem. Soc. R. Sci. Liege*, 6, ser., **10:** 141-164.

Flather, R.A., 1979. Recent results form a storm surge prediction scheme for the North Sea, in Marine Forecasting, ed. Nihoul, J.C.J., *Proc. 10th Int. Liege Coll. Ocean Hydrodynamics,* 1978, 385-409.

Flather, R.A. and Davies, A.M., 1978. On the specification of meteorological in numerical modesl for North Sea storm surge prediction, with application to the surge of 2 to 4 January 1976, Dt. hydrogr. Z. Erganzungsheft, A. No. 15, 51.

Flather, R.A. and Heaps, N.S., 1975. Tidal computation for Morecambe Bay, *Geophys. J.R., Astr. Soc.,* **42:** 489-517.

Fu, L.L., 1983. Recent progress in the application of satellite altimetry to observing the mesoscale variability and general circulation of the oceans, *Rev. Geophys. Space Phys.,* **21:** 1657-1666.

Garratt, J.R., 1977. Review of drag coefficient over oceans and continents, *Mon. Weather Rev.,* **105:** 915-929.

Grace, S.F., 1930. The influence of friction on the tidal motion of the Gulf of Suez, *Mon. Notic. Roy. Astron. Soc., Geophys.* Suppl., 2, 316.

Grace, S.F., 1931. The influence of firction on the tidal motion of the Gulf of Suez, *Mon. Notic. Roy. Astron. Soc., Geophys.* Suppl., 7, 309-318.

Groen, P. and Groves, G.W., 1962. Surges, in The Sea, **1:** 611-646, e.d. Hill, M.N., Wiley, New York.

Hasse, L. and Wagner, V., 1971. On the relationship between geostrophic and surface wind on sea, *Mon. Weather Rev. Wash.,* **99:** 225-260.

Heaps, N.S., 1965. Storm surge on continental shelf, *Phil. Trans. R. Soc., A,* **257:** 351-383.

Heaps, N.S., 1969. A two-dimenisional numerical sea model, *Phil. Trans. R. Soc., A,* **265:** 93-137.

Heaps, N.S., 1983. Strom surges, 1967-1982. *Geophys. J.R., Astr. Soc.,* **74:** 331-376.

Heaps, N.S. and Jones, J.E., 1979. Recent storm surge in Irish sea, Marine Forecasting, Elsevier Scientific Publishing Company.

Heathershaw, A.D., 1976. Measurement of turbulence in the Irish Sea benthic boundary layer, in The Benthic Boundary Layer, ed. McCave, I.N., Plenum Press, N.J., 11-31.

Hsueh, Y. and Romea, R.D., 1983. Romea, A. comparison of observed and geostrophically calculated wintertime surface wind over the East China Sea, *J. Geophys. Res.,* **88:** C14, 9588-9594, 1983.

Kinsman, B., 1965. Wind Waves, Prentice Hall Inc., Englewood Cliffs, N.J.

Lambeck, K., 1975. Effects of tidal disspation in the oceans on the Moon's orbit and the Earth's rotation. *J. Geophys. Res.,* **80:** 2917-2925.

Large, W.G., 1979. The turbulent fluxes of momentum and sensible heat over the open sea during moderate to strong wind, Ph.D. thesis. Univ. of British Columbia, Vancouver, Canada.

Larson, L.H. and Cannon, G.A., 1983. Tides in the East China Sea, Paper presented to the Symposium on sedimentation on the continental shelf, Hangzhon, China.

Le Provost, C., 1983. An analysis of SEASAT altimeter measurements over a coastal area: The English Channel, *J. Geophys. Res.,* **88:** C3, 1647-1754.

Lerch, F.J., C.A. Wagner, S.M. Klosko, and Putney, B.H., 1981. Goddard earth models for oceanographic applications (GEM 10B and 10C), *Marine Geodesy,* **5**(2): 2-43.

Marsh, J.G. and Martin, T.V., 1982. The SEASAT altimeter mean sea surface model, *J. Geophys. Res.,* **87:** C5, 3269-3280.

Marsh, J.G. and Williamson, R.G., 1980. Precision orbit analyses in support of the SEASAT altimeter experiment. *J. Astronaut. Sci.,* **XXVIII**(4): 345-369.

Moon, W. and Tang, R., 1984. On the hydrodynamic correction of SEASAT altimeter data (Hudson Bay area of Canada), Marine Geodesy.

Munk, W.H. and MacDonald, G.J.F., 1960. The Rotation of the Earth, a geophysical discussion, Cambridge University Press.

Parke, M.E. and Hendershott, M.C., 1980. M2, S2, K1 models of the global ocean tide on an elastic earth, *Marine Geodesy,* vol. 3, 379-408.

Powell, M.D., 1980. Evaluations of diagnostic marine boundary-layer model applied to hurricanes, *Mon. Weather Rev.,* **108:** 757-766.

Pekeris, C.L. and Accad, Y., 1969. Solution of Laplace's equation for the M2 tide in the world oceans, *Phil. Trans. Roy. Soc.* London, A265, 413.

Ramming, H.G., 1978. Numerical investigation of the influence of coastal structures upon the dynamic offshore process by application of a nested tidal model, in Hydrodynamics of Estuaries and Fjords, ed. Nihoul, J.C.J., Elsevier Oceanography Series 23.

Roberts, K.V. and Weiss, N.O., 1976. Convective difference schemes, *Math. Comput.,* **20:** 272-299.

Schwiderski, E.W., 1978. Global ocean tides, Part I: A detailed hydrodynamics interpolation model, NSWC/DL Tr-3866, Naval Surface Weapons Center, Dahlgren, Va.

Schwiderski, E.W., 1980. On charting global ocean tides, *Rev. of Geophys. and Space Phys.,* vol 18, 1.

Smith, S.D., 1980. Wind stress and heat flux over the ocean in gale force winds, *J. Phys. Oceanogr.,* **10:** 709-726.

Sternberg, R.W., 1968. Friction factors in tidal channels with differing bed roughness, *Mar. Geol.,* **6:** 243-260.

Stock, G.G., 1976. Modelling of tides and tidal dissipation in the Gulf of Californi, Ph.D. dissertation, Universi-

ty of California, San Diego.

Tang, R., 1984. Ocean bottom friction study using hydrodynamic modelling and SEASAT-ALT data, M.Sc. thesis, University of Manitoba, Winnipeg, Manitoba.

Tang, R. and Moon, W., 1984. Finite difference transient sea surface modelling for the SEASAT altimeter data correction, Congressus Numerantium, Vol. 42, 299-312.

Weatherly, G.L. and Wimbus, M., 1980. Near-bottom speed and temperature observations on the Blake-Bahama Outer Ridge, *J. Geophys. Res.*, **85:** 3971-3981.

Weenink, M.P.H., 1958. A theory and method of calculation of wind effects on sea levels in a partly-enclosed sea, with special application to the southern coast of the North Sea, Koninklijk Nederlands Meterologisch Institude, Mededelingen en Verhandelingen, 73.

Wolf, J., 1980. Estimation of the shearing stress in a tidal current with application to the Irish Sea, in Marine Turbulence, ed., Nihoul, J.C.J., Elsevier Oceanography Series 28.

Wu, J., 1969. Wind stress and surface rougness at air-sea interface, *J. Geophys. Res.*, **74:** 444-455.

Wu, M., 1980. Wind-stress coefficients over sea surface near neutral conditions: A revisit, *J. Phys. Oceanogr.*, **10:** 727-247.

Wu, J., 1982. Wind-stress coefficients over sea surface from breeze to hurricane, *J. Geophys. Res.*, **C12:** 9704-9706.